Cement and Concrete Research 172 (2023) 107237

Contents lists available at ScienceDirect

Cement and Concrete Research

journal homepage: www.elsevier.com/locate/cemconres

# Mix-, storage- and temperature-invariant precipitation characteristics in white cement paste, expressed through an NMR-based analytical model

Nabor Jiménez Segura, Bernhard L.A. Pichler, Christian Hellmich *

*Institute for Mechanics of Materials and Structures, TU Wien (Vienna University of Technology), Karlsplatz 13/202, 1040 Vienna, Austria*

ARTICLE INFO

*Keywords:*
Cement paste
NMR
Hydration
Kinetics
Micromechanics modeling

ABSTRACT

Proton NMR tests on hydrating white cement paste provide access to the mix-, storage-, and temperature-dependent evolutions of the hydrogen portions found in capillary and gel pores, solid C-S-H, and calcium hydroxide, respectively. The aforementioned dependencies vanish once the hydrogen molar fractions are plotted as functions of the precipitation degree, which we have introduced here as the ratio of the amount of hydrogen bound in solids, over the total amount of hydrogen. The precipitation rate is governed by one activation energy and a linear affinity function of the current precipitation degree normalized by its maximum value. The latter decreases linearly with increasing curing temperature, being consistent with the temperature-dependent water content of solid C-S-H. The corresponding water-to-silica ratio, together with the precipitation degree and the mix and storage characteristics, provide access to the volume fractions of the hydrogen-containing phases, of clinker, and of voids, as well as to the degree of hydration.

## 1. Introduction

Cement hydration [1] comprises a number of chemical reactions between water and different clinker components [with the most prominent ones being tricalcium silicate or alite, with chemical formula $(CaO)_3(SiO_2)$ or, in short, $C_3S$, and dicalcium silicate or belite, with chemical formula $(CaO)_2(SiO_2)$ or, in short, $C_2S$], leading to the formation of hydration products [with the most prominent ones being calcium-silicate-hydrate, with chemical formula $(CaO)_x(SiO_2)(H_2O)_y$ or, in short, solid C-S-H, and calcium hydroxide or portlandite, with chemical formula $Ca(OH)_2$ or, in short, CH]. More explicitly, when not differentiating between the individual reactants and the individual products, a single chemical equation appears as appropriate, reading as

$$clinker + water \rightarrow hydration\ products\,. \tag{1}$$

In this context, one may add that Eq. (1) is strictly fulfilled only at the end of the hydration reaction of mixes with a "stiochiometric value" [2] of the (initial) water-to-cement (mass) ratio amounting to $w/c = 0.42$. Then, clinker and water are completely transformed into hydration products. In the case of $w/c < 0.42$, some *clinker* would be left on the right-hand side of the reaction; and in the case of $w/c > 0.42$, some (capillary) *water* would be left on the right-hand side of the reaction [2]. The kinetics associated with Eq. (1) is traditionally monitored by means of the degree of hydration, $\xi$, a standard definition of which is the following [2–7]

$$\xi(t) = 1 - \frac{m_{clin}(t)}{m_{clin}(t=0)}\,, \tag{2}$$

with $m_{clin}$ standing for the mass of clinker and $t$ denoting the age of the material.

However, Eq. (1) conceals that the chemical reactions between clinker and water, resulting in the formation of hydration products falls into (at least) two processes [8–12]: (i) the (exothermic) dissolution of clinker, providing an ionic solution; and (ii) the precipitation of the hydration products (mainly calcium-silicate-hydrate and calcium hydroxide) out of the aforementioned ionic solution. When focusing on the latter precipitation process, a radically simple chemical reaction equation may be adopted, namely

$$\mathrm{H}^{HM} \rightarrow \mathrm{H}^{LM}\,, \tag{3}$$

with H standing for the hydrogen atoms, highly mobile ($HM$) in the ionic solution, and bound (and hence with low mobility - $LM$) in solid C-S-H or CH. A particularly interesting feature of the precipitation equation, Eq. (3), is that its kinetics can be followed from proton nuclear magnetic resonance relaxometry (proton NMR). This technique delivers $T_2$ relaxation times which quantify the decay of a magnetic signal associated with the movement of hydrogen atoms. In more detail,

* Corresponding author.
*E-mail address:* Christian.Hellmich@tuwien.ac.at (C. Hellmich).

https://doi.org/10.1016/j.cemconres.2023.107237
Received 30 June 2022; Received in revised form 9 June 2023; Accepted 20 June 2023
Available online 7 July 2023

hydrogen atoms in cement paste fall into four mobility classes associated with four typical relaxation times: (i) stronger chemical bonding in crystals such as calcium hydroxide, (ii) weaker chemical bonding in calcium-silicate-hydrate building blocks (solid C-S-H), (iii) stronger confinement in gel pores, and (iv) weaker confinement in capillary pores. As regards terminology, the composite made of solid C-S-H building blocks and gel pores is referred to as the "C-S-H gel" [13–15]. In the existing literature, water bound in solid C-S-H is also referred to as "interlayer water" [16], gel pores as "intra-C-S-H pores" [16], and capillary pores as "inter-C-S-H pores" [16] as well as "interhydrate pores" [17], respectively. The essential result of one proton NMR test are four signal intensities. Their sum is referred to as the "total signal intensity".

The evolution of the total signal intensity depends on the storage conditions. It is constant under sealed conditions [17,18], because no hydrogen enters or leaves the tested specimen, see Fig. 1 for pastes with different $w/c$ ratios. As regards cement pastes being cured under water, however, the total signal intensity increases with increasing material age [19,20], because of uptake of water, see Fig. 2 for pastes cured at different temperatures. This water fills the space which emerges as the hydration products fill a smaller volume than the reactants they are made of (i.e. a smaller volume than that originally filled by clinker and water). The latter phenomenon is usually referred to as chemical shrinkage [21,22]. Under sealed conditions, in turn, chemical shrinkage results in a progressively increasing hydrostatic tension of the porewater. This tension causes water to cavitate [23], which leads to the creation of voids filled by water vapor. Their volume fraction increases with increasing material maturation [11,12].

The experimental data illustrated in Figs. 1 and 2, associated to clinkers with mineralogical compositions given in Table 1, are the basis for the present analysis, dealing with the quantification of the precipitation process in terms of differently mobile hydrogen fractions. As a naturally emerging quantity describing exactly this precipitation in the context of proton NMR data, we resort to the amount of solidly bound hydrogen (i.e. that with relaxation times of $T_2 \approx 100\,\mu s$ and smaller [24]), and relate it to the overall hydrogen (irrespective of its mobility). Accordingly, we here coin the term of "precipitation degree" $\eta$ as

$$\eta = \frac{\mathrm{H}^{LM}}{\mathrm{H}^{HM}+\mathrm{H}^{LM}} = \frac{a_{H,CH}+a_{H,sCSH}}{a_H}\,, \tag{4}$$

with $a_{H,CH}$ and $a_{H,sCSH}$ standing for the amounts of hydrogen bound into calcium hydroxide ($CH$) and into solid C-S-H ($sCSH$), respectively, and with $a_H$ as the total amount of hydrogen found in the tested sample at the time of testing, including both solidly bound hydrogen and hydrogen in liquid form, the latter filling either the gel ($gpor$) or the capillary pores ($cpor$): $a_H = a_{H,CH} + a_{H,sCSH} + a_{H,gpor} + a_{H,cpor}$. As a function of this newly introduced precipitation degree, we will study paste composition, reaction kinetics, as well as the evolution of the mass density of solid C-S-H, and we will finally link all the insight gained here to the key quantity of traditional cement chemistry: the degree of hydration according to Eq. (2). Accordingly, the remainder of the present paper is organized as follows: Section 2 covers the evolution of the amounts of differently bound hydrogen portions; and then elucidates characteristics which are independent of initial composition, curing temperature, and storage conditions. The temperature-independent aspects of the precipitation kinetics are quantified in Section 3, in terms of an affinity function depending on a normalized precipitation degree only, while temperature intervenes through an Arrhenius-type activation term. Section 4 translates the molar fractions of hydrogen into masses, linking the precipitation degree to the classical hydration degree. Section 5 translates these masses into phase-evolution diagrams, providing volume fractions of gel and capillary porosities, calcium hydroxide, and solid C-S-H, together with the ones of clinker and vapor-filled voids as functions of the precipitation degree. Then, Section 6 (Discussion and Conclusion) puts the novel results in context with the current state of the art.

**Table 1**
Phase composition (in weight-%) of the batches of white cement from Aalborg Portland used for pastes cured under sealed conditions [18] and under water [19].

| Phases | Sealed curing | Underwater storage | |
|---|---|---|---|
| | batch 1 | batch 1 | batch 2 |
| alite | 66.9 | 66.9 | 64.0 |
| belite | 20.0 | 19.7 | 19.5 |
| aluminate | 3.5 | 3.6 | 3.3 |
| ferrite | 1.0 | 0.8 | 0.0 |
| calcium hydroxide | 1.0 | 0.7 | 1.8 |
| anhydrite | 2.3 | 2.6 | – |
| bassanite | 2.1 | 2.1 | 2.1 |
| lime | 0.3 | – | – |
| gypsum | – | – | 3.3 |
| amorphous | 2.9 | 3.6 | 6.0 |

## 2. Temperature-, storage-, and mix-invariant relations between molar fractions of differently mobile hydrogen portions and the precipitation degree $\eta$

### 2.1. Normalized NMR signals, molar fractions of differently mobile hydrogen portions, and the precipitation degree

Muller et al. [17,18] and Gajewicz et al. [19,20] published normalized NMR signals intensities:

$$I_j(t) := \frac{S_{H,j}(t)}{S_H(t=0)}\,, \qquad j \in [CH, sCSH, gpor, cpor]\,, \tag{5}$$

see Figs. 1 and 2. $S_{H,j}$ stands for the signal intensity associated with hydrogen in calcium hydroxide, solid C-S-H, gel pores, and capillary pores, $S_H$ for the total signal intensity, $t$ for the time, and $t=0$ for the time instant of the first NMR measurement. $S_{H,j}$ is proportional to the amount of hydrogen in material domain $j$, while $S_H$ is proportional to the total amount of hydrogen in the tested sample of cement paste. Therefore, Eq. (5) can be re-written in terms of amounts of hydrogen:

$$I_j(t) = \frac{a_{H,j}(t)}{a_H(t=0)}\,, \qquad j \in [CH, sCSH, gpor, cpor]\,. \tag{6}$$

Eq. (6) allows for expressing $\eta$ according to Eq. (4) as:

$$\eta(t) = \frac{I_{CH}(t)+I_{sCSH}(t)}{I_{CH}(t)+I_{sCSH}(t)+I_{gpor}(t)+I_{cpor}(t)}\,. \tag{7}$$

Notably, the precipitation degree according to Eq. (4) relates the amount of solidly bound hydrogen, at any time $t$, to the total amount of hydrogen which is in the system *at that time*, rather than to the initial amount of hydrogen. This provides the motivation to introduce the molar fractions of the differently bound hydrogen portions

$$\mathcal{F}_{H,j}(t) := \frac{a_{H,j}(t)}{a_H(t)}\,, \qquad j \in [CH, sCSH, gpor, cpor]\,, \tag{8}$$

where, differing from the situation encountered in Eqs. (5) and (6), $a_H(t)$ rather than $a_H(t=0)$ appears in the denominator. Therefore, the sum of all four different hydrogen molar fractions is, at any time $t$, equal to 1:

$$1 = \mathcal{F}_{H,CH}(t) + \mathcal{F}_{H,sCSH}(t) + \mathcal{F}_{H,gpor}(t) + \mathcal{F}_{H,cpor}(t)\,. \tag{9}$$

The corresponding expression for the precipitation degree $\eta$ as a function of the molar fractions of the differently mobile hydrogen portions is obtained from inserting Eq. (8) into Eq. (4), yielding

$$\eta(t) = \mathcal{F}_{H,CH}(t) + \mathcal{F}_{H,sCSH}(t)\,. \tag{10}$$

Insertion of Eq. (10) into Eq. (9) allows one to express the molar fraction of hydrogen in liquid form, as function of the precipitation degree:

$$1 - \eta(t) = \mathcal{F}_{H,gpor}(t) + \mathcal{F}_{H,cpor}(t)\,. \tag{11}$$

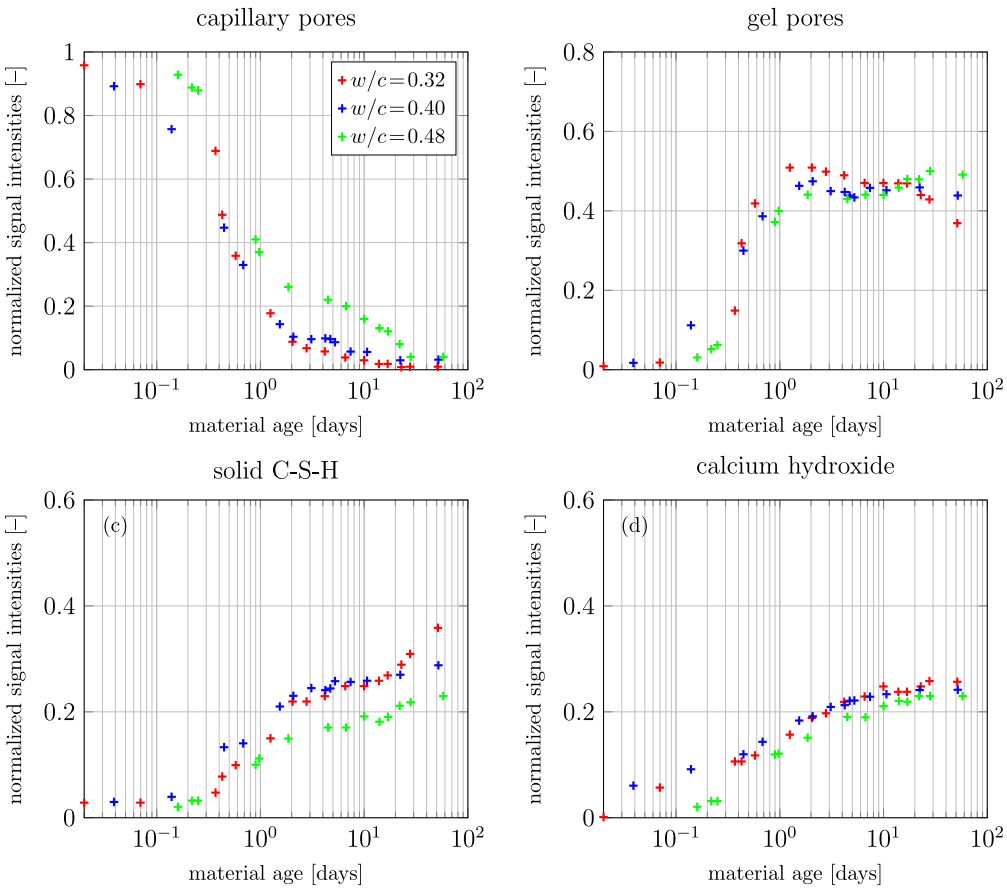


**Fig. 1.** Proton NMR signal fractions as function of material age, obtained from white cement paste samples of 8 mm diameter and 10 mm height, with $w/c=0.32$ (red), $w/c=0.40$ (blue), and $w/c=0.48$ (green), cured under sealed conditions at $T=20$ °C [17,18]: normalized signal intensities of hydrogen (a) in capillary pores ($cpor$), (b) in gel pores ($gpor$), (c) in solid C-S-H ($sCSH$), and (d) in calcium hydroxide ($CH$). (For interpretation of the references to color in this figure legend, the reader is referred to the web version of this article.)

### *2.2. Identification of mix-invariant relations between hydrogen molar fractions and precipitation degree; obtained from NMR data of samples cured under sealed conditions*

Sealed samples are closed systems. The total amount of hydrogen is constant over time, and equal to the initial amount: $a_H(t) = a_H(t=0)$, and the same holds for the total NMR signal intensity: $S_H(t) = S_H(t=0)$. Therefore, the molar fractions of the differently mobile hydrogen portions according to Eq. (8) are equal to the normalized NMR signals according to Eqs. (5) and (6), see Fig. 1 for experimental data:

$$\mathcal{F}_{H,j}(t) = I_j(t)\,, \qquad j \in [CH, sCSH, gpor, cpor]\,. \tag{12}$$

A parametric plot showing the molar fraction of hydrogen in solid C-S-H over the precipitation degree, produced from the normalized NMR signal intensities from Fig. 1, in combination with Eqs. (7) and (12), underlines that $\mathcal{F}_{H,sCSH}$ increases overlinearly with increasing $\eta$, independently of the initial water-to-cement mass ratio, see Fig. 3. This overlinear trend can be quantified by means of a power law:

$$\mathcal{F}_{H,sCSH} = \pi_1\,\eta^{\pi_2}\,, \tag{13}$$

with the numerical values of the constants $\pi_1$ and $\pi_2$ being listed in Table 2. The mathematical relation between the molar fraction of hydrogen in calcium hydroxide and the precipitation degree is obtained from inserting Eq. (13) into Eq. (10), and from solving the resulting expression for $\mathcal{F}_{H,CH}$:

$$\mathcal{F}_{H,CH} = \eta - \pi_1\,\eta^{\pi_2}\,. \tag{14}$$

**Table 2**
Factorial, exponential, and proportionality constants quantifying mix-, storage-, and temperature-independent precipitation characteristics, identified from the NMR data of Fig. 1.

| Context | Value of the constant | References |
|---|---|---|
| precipitation of solid C-S-H | $\pi_1 = 0.6419$ | Eq. (13), Fig. 3 |
| precipitation of solid C-S-H | $\pi_2 = 1.3000$ | Eq. (13), Fig. 3 |
| development of gel and capillary pores | $\pi_3 = 1.9095$ | Eq. (19), Fig. 4 |

In order to differentiate, within the total water-filled pore space, between gel and capillary pores, volume fractions of gel and capillary pores with respect to the total pore volume are introduced as:

$$\varphi_{gpor}(t) = \frac{\mathcal{F}_{H,gpor}(t)}{\mathcal{F}_{H,cpor}(t) + \mathcal{F}_{H,gpor}(t)}\,, \tag{15}$$

$$\varphi_{cpor}(t) = \frac{\mathcal{F}_{H,cpor}(t)}{\mathcal{F}_{H,cpor}(t) + \mathcal{F}_{H,gpor}(t)}\,, \tag{16}$$

such that $\varphi_{gpor}(t)+\varphi_{cpor}(t) = 1$. Illustrating $\varphi_{gpor}(t)$ and $\varphi_{cpor}(t)$ according to Eqs. (15) and (16) over $\eta(t)$, based on NMR signals from Fig. 1 as well as Eqs. (7) and (12), evidences a virtually linear dependence of both $\varphi_{cpor}$ and $\varphi_{gpor}$, on the precipitation degree, with decreasing and increasing trends, respectively, and independent of the initial water-to-cement mass ratio, see Fig. 4. The point-wisely resolved relationship is reproduced by means of the following bilinear functions:

$$\varphi_{gpor} = \begin{cases} \pi_3\,\eta \;\ldots\; \eta \le 1/\pi_3\,, \\ 1\;\;\ldots\; \eta > 1/\pi_3\,, \end{cases} \tag{17}$$

$$\varphi_{cpor} = \begin{cases} 1-\pi_3\,\eta \;\ldots\; \eta \le 1/\pi_3\,, \\ 0\;\;\ldots\; \eta > 1/\pi_3\,, \end{cases} \tag{18}$$

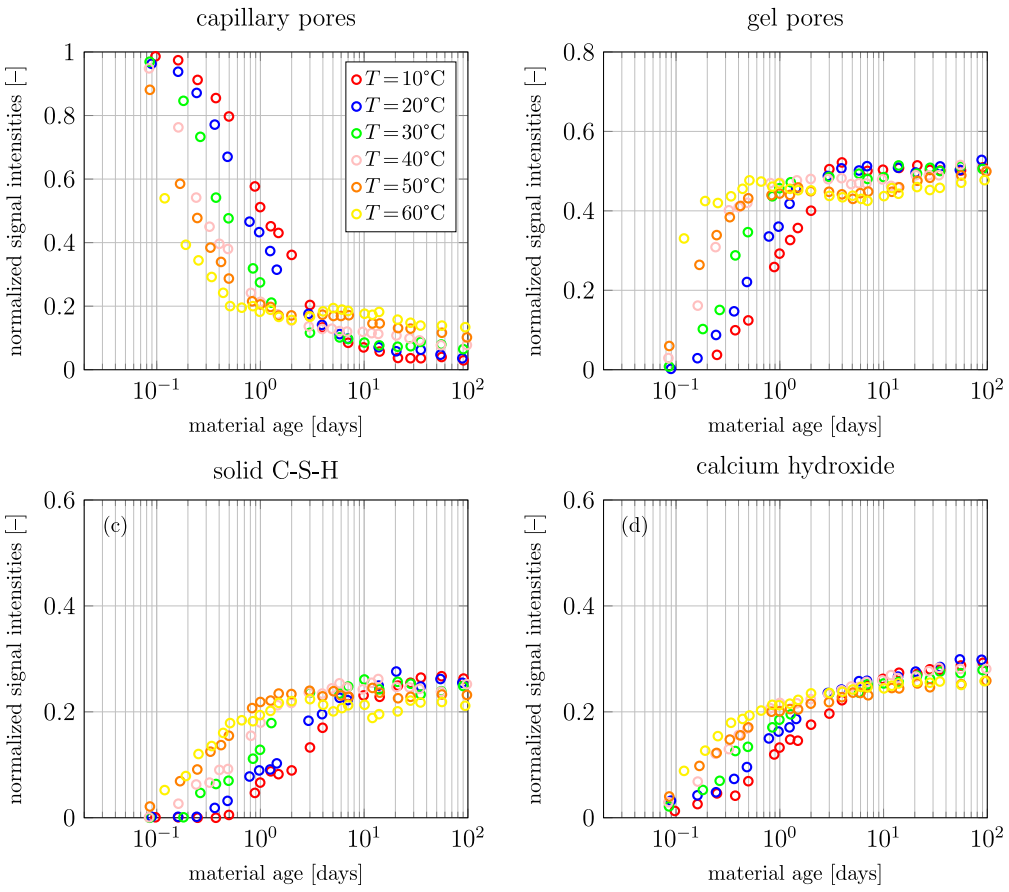


**Fig. 2.** Proton NMR signal fraction as function of material age, obtained from white cement paste samples of 8 mm diameter and 10 mm height, with $w/c = 0.40$ and cured under water at different temperatures [19,20]: $T = 10$ °C (red), $T = 20$ °C (blue), $T = 30$ °C (green), $T = 40$ °C (pink), $T = 50$ °C (orange), and $T = 60$ °C (yellow): normalized signal intensities of hydrogen in (a) capillary pores (*cpor*), (b) gel pores (*gpor*), (c) solid C-S-H ($sCSH$), and (d) calcium hydroxide ($CH$). (For interpretation of the references to color in this figure legend, the reader is referred to the web version of this article.)

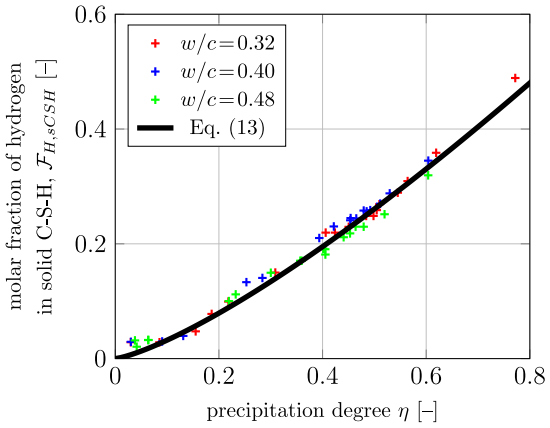


**Fig. 3.** Molar fraction of hydrogen in solid C-S-H, $\mathcal{F}_{H,sCSH}$, as function of the precipitation degree $\eta$: the points are derived from NMR data of Fig. 1, the solid line refers to the power-law of Eq. (13), with constants listed in Table 2. (For interpretation of the references to color in this figure legend, the reader is referred to the web version of this article.)

with the numerical value of the constant $\pi_3$ being listed in Table 2. The mathematical relation between $\mathcal{F}_{H,gpor}$, the molar fraction of hydrogen in gel pores, and $\eta$ is obtained from solving Eq. (15) for $\mathcal{F}_{H,gpor}$ and from inserting Eqs. (11) and (17) into the resulting expression, yielding

$$\mathcal{F}_{H,gpor} = \begin{cases} (1-\eta)\,(\pi_3\,\eta)\ \ldots & \eta \le 1/\pi_3\,, \\ 1-\eta\ \ldots & \ldots\ \eta > 1/\pi_3\,. \end{cases} \tag{19}$$

Similarly, the mathematical relation between $\mathcal{F}_{H,cpor}$, the molar fraction of hydrogen in capillary pores, and $\eta$ follows as

$$\mathcal{F}_{H,cpor} = \begin{cases} (1-\eta)\,(1-\pi_3\,\eta)\ldots & \eta > 1/\pi_3\,, \\ 0\ \ldots\ldots & \ldots\ \eta > 1/\pi_3\,. \end{cases} \tag{20}$$

Eqs. (13), (14), (19), and (20) quantify the four different molar fractions of hydrogen, as functions of the precipitation degree, independently of the initial water-to-cement mass ratio, see Fig. 5. In order to check whether Eqs. (13), (14), (19), and (20) are also independent of curing temperature and storage conditions, the NMR data of Gajewicz et al. [19,20] will be analyze next, see also Appendix for further details on the essentials concerning tested materials and testing procedures.

### *2.3. Testing temperature- and storage-invariance of the relations between hydrogen molar fractions and the precipitation degree: evaluation of NMR data from samples cured under water at six different temperatures*

Samples cured under water are open systems. Driven by chemical shrinkage, water is sucked into the open porosity of the samples. This results in a progressive increase of the total amount of hydrogen in the sample, as indicated by the total NMR intensity. Under these conditions, the molar fractions of hydrogen according to Eq. (8) are equal to normalized signal intensities according to Eqs. (5) and (6), divided by the sum of all four normalized signal intensities:

$$\mathcal{F}_{H,j}(t) = \frac{I_j(t)}{I_{CH}(t) + I_{sCSH}(t) + I_{gpor}(t) + I_{cpor}(t)}\,, \quad j \in [CH, sCSH, gpor, cpor]\,. \tag{21}$$

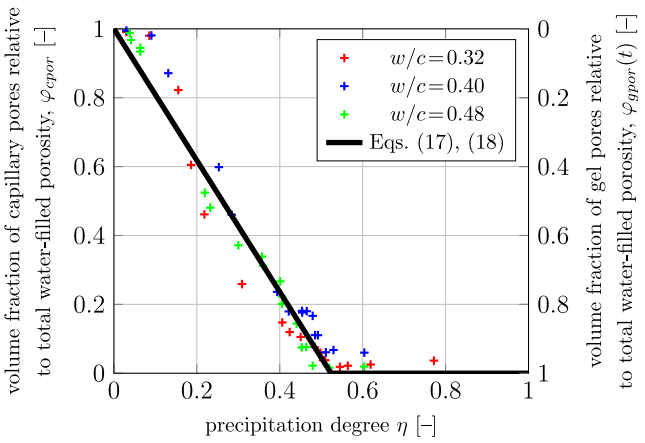


**Fig. 4.** Trends of gel and capillary pore fractions, with the precipitation degree: the points are derived from NMR data of Fig. 1, the solid line refers to the bilinear function of Eqs. (17) and (18), see also Table 2. (For interpretation of the references to color in this figure legend, the reader is referred to the web version of this article.)

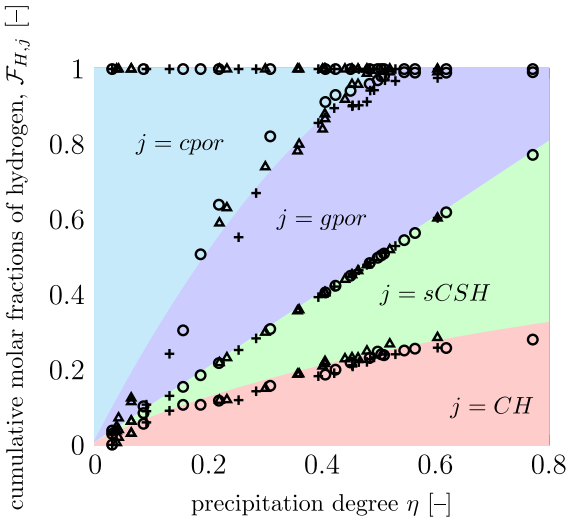


**Fig. 5.** Cumulative molar fractions of hydrogen found in capillary pores ($cpor$), gel pores ($gpor$), solid C-S-H ($sCSH$), and calcium hydroxide ($CH$), as functions of the precipitation degree: the data points refer to NMR data from sealed-cured cement pastes with different initial water-to-cement mass ratios [17,18]: $w/c$ = 0.32 (circles), $w/c$ = 0.40 (crosses), and $w/c$ = 0.48 (triangles); the shaded domains refer to hydrogen in calcium hydroxide ($CH$, pink), solid C-S-H ($sCSH$, green), gel pores ($gpor$, purple), and capillary pores ($cpor$, blue); the boundaries between the shaded domains refer to Eqs. (13), (14), (19), and (20), together with the constants of Table 2. (For interpretation of the references to color in this figure legend, the reader is referred to the web version of this article.)

Inserting the NMR data from Fig. 2 into Eqs. (7) and (21) allows for illustrating the evolution of molar fractions of hydrogen as a function of the precipitation degree, see the points in Fig. 6. The obtained chains of data points referring to NMR data of under water cured samples agree well with the model predictions derived from samples cured under sealed conditions, according to Eqs. (13), (14), (19), and (20), together with the constants of Table 2; these predictions being indicated through the boundaries between the differently shaded domains in Fig. 6.

Notably, the boundaries between the differently shaded phase domains in Figs. 5 and 6 are the same. The data points, in turn, come from two different laboratories and refer to two different NMR testing devices, two different cements, three different values of the initial water-to-cement mass ratio, six different values of the curing temperature, and two different types of storage conditions. Thus, Figs. 5 and 6 corroborate the remarkable "universality" of the Eqs. (13), (14), (19), and (20), see also Table 2. These relations are independent of initial composition, curing temperature, and storage conditions.

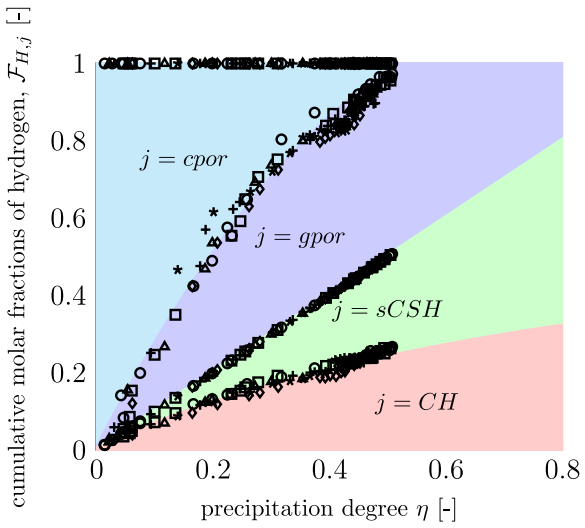


**Fig. 6.** Exemplary model validation: cumulative molar fractions of hydrogen as function of the precipitation degree: the data points refer to NMR data from under water cured cement pastes stored at different temperatures [19,20]: $T$ = 10 °C (circles), $T$ = 20 °C (squares), $T$ = 30 °C (triangles), $T$ = 40 °C (crosses), $T$ = 50 °C (diamonds), and $T$ = 60 °C (stars); the shaded domains refer to hydrogen in calcium hydroxide ($CH$, pink), solid C-S-H ($sCSH$, green), gel pores ($gpor$, purple), and capillary pores ($cpor$, blue); the boundaries between the shaded domains are model-predictions according to Eqs. (13), (14), (19), and (20), together with the constants of Table 2. (For interpretation of the references to color in this figure legend, the reader is referred to the web version of this article.)

**Table 3**
Temperature-independent binary variable $\pi_4$ distinguishing between two types of curing conditions: (i) sealed storage (= closed system), and (ii) underwater storage (= open system), leading to the increase of the total amount of hydrogen resulting from uptake of water driven by chemical shrinkage.

| Curing conditions | Value of the binary variable |
|---|---|
| sealed storage | $\pi_4 = 0.0000$ |
| underwater storage | $\pi_4 = 0.1880$ |

### 2.4. Water and hydrogen uptake characteristics of cement pastes cured under water

Cement pastes cured under water suck in water in order to fill the space provided by chemical shrinkage (Le Châtelier contraction). It is instructive to plot the corresponding hydrogen uptake normalized by the initial hydrogen amount, $\Delta I_H$, which reads, under consideration of Eq. (6), as

$$\Delta I_H(t) = \frac{a_H(t) - a_H(t=0)}{a_H(t=0)} = \frac{I_{tot}(t) - I_{tot}(t=0)}{I_{tot}(t=0)}, \tag{22}$$

with $I_{tot}(t) = I_{CH}(t) + I_{sCSH}(t) + I_{gpor}(t) + I_{cpor}(t)$, as function of the precipitation degree, see Fig. 7. One observes that also the hydrogen-uptake of cement pastes cured under water turns out as a temperature-independent linear precipitation characteristic, which can be mathematically quantified as

$$\forall t: \quad \Delta I_H(t) = \pi_4\, \eta(t), \quad \rightarrow \quad \Delta I_H = \pi_4\, \eta = \frac{a_H(\eta) - a_H(\eta=0)}{a_H(\eta=0)}, \tag{23}$$

with the numerical value of the constant $\pi_4$ being listed in Table 3.

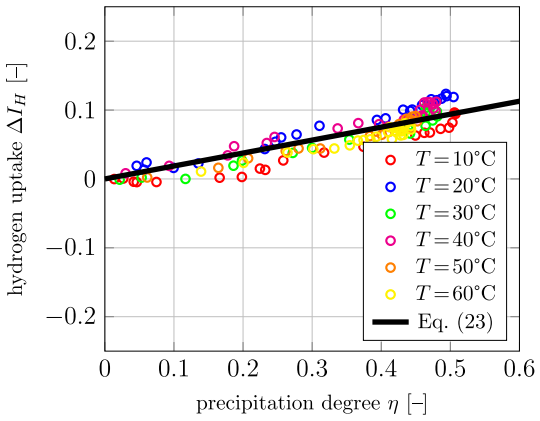


**Fig. 7.** Relative increase of the total NMR intensity (reflecting water uptake by cement pastes cured under water) as function of the precipitation degree; the points are derived from the NMR data of Fig. 2, the solid line refers to the linear function of Eq. (23), see also Table 3. (For interpretation of the references to color in this figure legend, the reader is referred to the web version of this article.)

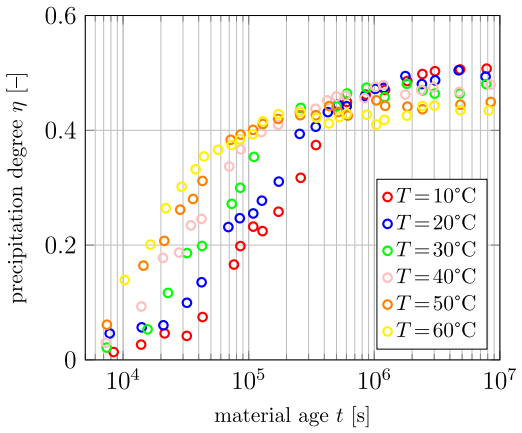


**Fig. 8.** Temporal evolution of the precipitation degree of cement pastes with $w/c = 0.40$ cured under water and isothermally at: $T = 10$ °C (red), $T = 20$ °C (blue), $T = 30$ °C (green), $T = 40$ °C (pink), $T = 50$ °C (orange), and $T = 60$ °C (yellow); the points were obtained from insertion of the data of Fig. 2 into Eq. (7). (For interpretation of the references to color in this figure legend, the reader is referred to the web version of this article.)

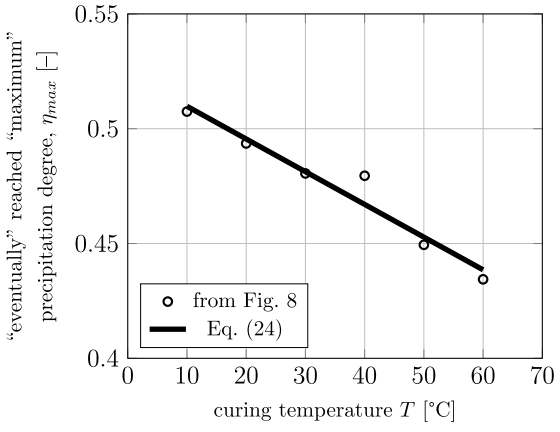


**Fig. 9.** "Eventually" reached "maximum" precipitation degree of cement pastes with $w/c = 0.40$ cured under water at different temperatures; the points refer to the rightmost data points in Fig. 8, the line refers to the best linear regression function, see Eq. (24) and Table 4.

**Table 4**
Constants quantifying the influence of temperature on the precipitation kinetics.

| Context/quantity | Value of the constant | Reference |
|---|---|---|
| slope in Fig. 9 | $\pi_5 = -1.425 \times 10^{-3}$ °C$^{-1}$ | Eq. (24) |
| intercept in Fig. 9 | $\pi_6 = 0.5240$ | Eq. (24) |
| reference water-to-silica ratio | $[(H_2O)/(SiO_2)](T = 20$ °C$) = 1.8$ | [17,25] |
| activation energy | $E_a = 33.260$ kJ/mol | [26,27] |
| universal gas constant | $R = 8.3145$ J/(mol°C) | |
| chemical affinity function | $A_0 = 6.124$ s$^{-1}$ | Eq. (28) |

## 3. Precipitation kinetics

### 3.1. Precipitation evolutions governed by curing temperature, derived from NMR data

Translating, by means of Eq. (7), the NMR data of Fig. 2 into values of the precipitation degree, and illustrating them as a function of the age of the material, provides quantitative insight into remarkable features, as can be seen from Fig. 8: (i) at early age, the precipitation process is the faster, the higher the curing temperature, (ii) at mature material ages, the reaction kinetics decays by orders of magnitude, such that the precipitation degree reaches a virtually constant value, and (iii) the "eventually" attained "maximum" precipitation degree, $\eta_{max}$, decreases with increasing curing temperature, in a virtually linear fashion, see Fig. 9.[1] The corresponding best linear regression function reads as

$$\eta_{max}(T) = \pi_5\, T + \pi_6\,, \tag{24}$$

with the numerical values of the constants $\pi_5$ and $\pi_6$ being listed in Table 4. The "eventually" attained "maximum" precipitation degrees of Fig. 9 suggests the introduction of a normalized precipitation degree, $\tilde{\eta}$, which increases from zero to one:

$$\tilde{\eta} = \frac{\eta}{\eta_{max}(T)}\,, \qquad 0 \le \tilde{\eta} \le 1\,. \tag{25}$$

It is important to note that the termination of the precipitation degree evolution at an ever lower value for increasing temperatures does not reflect kind of a premature termination of a chemical reaction, but rather a smaller amount of water in the same amount of solid C-S-H, as was evidenced by scanning electron microscopy, X-ray diffraction, and $Si^{29}$ NMR spectroscopy applied to cement paste samples cured at different temperatures [28]. Considering, accordingly, a water-to-silica ratio of 1.8 at $T = 20$ °C [17,25], the maximum precipitation degree of Eq. (24) proposes the former to decrease with increasing temperature in the form

$$[(H_2O)/(SiO_2)](T) = [(H_2O)/(SiO_2)](T = 20\ °C)\,\frac{\eta_{max}(T)}{\eta_{max}(T = 20\ °C)}$$
$$= 3.6327\big(\pi_5\, T + \pi_6\big)\,, \tag{26}$$

whereby we have made use of Eq. (24) and Table 4. The corresponding trend, illustrated in Fig. 10, agrees well with an independent testing campaign on oil-well cement, comprising X-ray diffraction with Rietveld analysis and thermogravimetry [29]; see Fig. 10. An even more "perfect" match between the solid line and the series of five data points in Fig. 10 is not necessarily expected, since the line and the points refer to different cements (white Portland cement versus oil-well cement), different hydration periods (100 versus 28 days), and different initial composition ($w/c = 0.40$ versus $w/c = 0.44$). Still, the accordance of trends seen in Fig. 10 strongly motivates the development of a kinetics model on the normalized precipitation degree according to Eq. (25), as described next.

[1] The words "eventually" and "maximum" were put under quotation marks, because, strictly speaking, hydration does never stop completely.

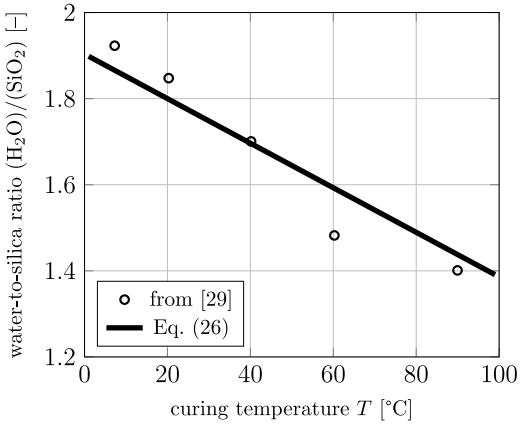


**Fig. 10.** Water-to-silica ratio of solid C-S-H: line computed from Eq. (26); data points from independent thermogravimetry [29].

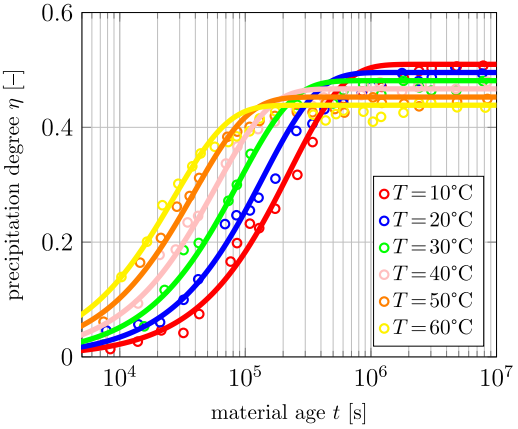


**Fig. 11.** Temporal evolution of the precipitation degree of cement pastes with $w/c = 0.40$ cured under water and isothermally at: $T = 10$ °C (red), $T = 20$ °C (blue), $T = 30$ °C (green), $T = 40$ °C (pink), $T = 50$ °C (orange), and $T = 60$ °C (yellow); the points were obtained from insertion of the data of Fig. 2 into Eq. (7), the solid lines were obtained from Eq. (31) and constants listed in Table 4. (For interpretation of the references to color in this figure legend, the reader is referred to the web version of this article.)

### 3.2. Identification of Arrhenius-type precipitation kinetics law

In line with pertinent hydration modeling on the basis of the degree of hydration [26,30–32], the evolution of $\tilde{\eta}$ is represented by an Arrhenius law [33]

$$\frac{\mathrm{d}\tilde{\eta}}{\mathrm{d}t} = A(\tilde{\eta})\,\exp\!\left(-\frac{E_a}{R\left[T(t)+273.15°\mathrm{C}\right]}\right), \tag{27}$$

where $A(\tilde{\eta})$ denotes the chemical affinity function, $E_a = 33.260\,\mathrm{kJ/mol}$ stands for the activation energy [26,27], and $R = 8.3145\,\mathrm{J/(mol°C)}$ the universal constant for ideal gases. $T(t)$ is the temporal evolution of the curing temperature in degrees centigrade. Analyzing *isothermal* NMR experiments, $T(t)$ becomes a constant.

As regards properties of $A(\tilde{\eta})$, Fig. 8 suggests that the chemical affinity function is positive for small values of $\tilde{\eta}$, and that it monotonously decreases with increasing $\tilde{\eta}$, approaching zero as $\tilde{\eta}$ approaches 1. From classical physical chemistry [34], a linear function is used:

$$A(\tilde{\eta}) = A_0\left(1-\tilde{\eta}\right), \qquad 0 \le \tilde{\eta} \le 1, \tag{28}$$

where $A_0$ is a constant which needs to be identified from experimental data. In order to derive a closed-form-solution for the time-evolution of $\tilde{\eta}$, Eq. (28) is inserted into Eq. (27). This delivers (under consideration of isothermal curing: $T$ = const.) a linear, inhomogeneous, ordinary, first-order differential equation with constant coefficients. Its solution reads as

$$\tilde{\eta} = 1 - \exp\!\left(-\frac{t}{t_0}\right), \tag{29}$$

where $t_0$ denotes a temperature-dependent characteristic time depending on $A_0$ and $T$, reading as

$$t_0 = \frac{1}{A_0}\exp\!\left(\frac{E_a}{R\left[T+273.15°\mathrm{C}\right]}\right). \tag{30}$$

A closed-form expression for the precipitation degree $\eta$ as a function of the age of the material and of the curing temperature is obtained from insertion of Eq. (30) into Eq. (29), from insertion of the resulting expression for $\tilde{\eta}$, together with Eq. (24), into Eq. (25), and from solving the obtained equation for $\eta$:

$$\eta_{mod} = \left[1-\exp\!\left(-t\,A_0\,\exp\!\left(-\frac{E_a}{R\left[T+273.15°\mathrm{C}\right]}\right)\right)\right]\times(\pi_5\,T+\pi_6), \tag{31}$$

where the subscript *mod* stands for "modeling".

For the identification of a value for $A_0$, and the subsequent checking of the significance of this value, we perform the following steps: First, we consider the NMR data associated with the experiments performed under the highest curing temperature: 60 °C. The following root-mean-square error function is minimized:

$$\epsilon(T) = \sqrt{\frac{1}{n_T}\sum_{i=1}^{n_T}\left[\eta_{mod}(T,t_i;A_0)-\eta_{exp}(T,t_i)\right]^2}, \tag{32}$$

where $n_T$ denotes the number of available experimental data points referring to curing temperature $T$, and where $\eta_{exp}(T,t_i)$ denotes *exp*erimental values resulting from insertion of NMR data of Fig. 2 into Eq. (7). The smallest attainable value of $\epsilon(60\ °\mathrm{C})$ amounts to 0.0182, and it is obtained for

$$A_0 = 6.124\,\mathrm{s}^{-1}, \tag{33}$$

see also the yellow graph and data points in Fig. 11.

**Table 5**
Root-mean-square errors according to Eq. (32), referring to the differences between experimental data points and Arrhenius-type kinetics model predictions of Fig. 11.

| $T$ | 10 °C | 20 °C | 30 °C | 40 °C | 50 °C | 60 °C |
|---|---|---|---|---|---|---|
| $\epsilon(T)$ | 0.0223 | 0.0260 | 0.0185 | 0.0171 | 0.0182 | 0.0182 |

Next, we evaluate Eq. (31) for the affinity value given in Eq. (33), together with the kinetics constants of Table 4, for the remaining curing temperatures of 10, 20, 30, 40, and 50 °C, see Fig. 11. The corresponding model curves agree remarkably well with the experimental data depicted in Figs. 8 and 11. Corresponding prediction errors according to Eq. (32) are satisfactorily small: even for the two smallest curing temperatures (10 °C and 20 °C, respectively) they are smaller than $1.5\times\epsilon(60\ °\mathrm{C})$, see Table 5. This underlines that *one* value of $A_0$, see Eq. (33), is sufficient for an appropriate description of the reaction kinetics, for curing temperatures ranging from 10 °C to 60 °C.

The NMR data, together with the validated kinetics model, provide a quantitative description of the following precipitation characteristics: the higher the curing temperature, the faster the reaction kinetics, but the smaller the finally attained precipitation degree [35], see Fig. 12. While the paste composition is solely governed by the precipitation degree, see Figs. 5 and 6, and while the precipitation kinetics can be described by one temperature-invariant chemical affinity function, see Eqs. (28) and (33) as well as Fig. 11, the "eventually" attained "maximum" precipitation degree does depend on the curing temperature. More precisely, it decreases with increasing curing temperature, see Figs. 11 and 12.

**Table 6**
Physical properties of water, calcium-silicate in C-S-H, and calcium hydroxide [17,25,28].

| | Water | Calcium-silicate in C-S-H | Calcium hydroxide |
|---|---|---|---|
| chemical formula | $H_2O$ | $(CaO)_{1.7}SiO_2$ | $Ca(OH)_2$ |
| hydrogen atoms per molecule [–] | $n_{H,H_2O} = 2$ | – | $n_{H,CH} = 2$ |
| molar mass [g/mol] | $M_{H_2O} = 18.01$ | $M_{CS} = 155.4$ | $M_{CH} = 74.09$ |

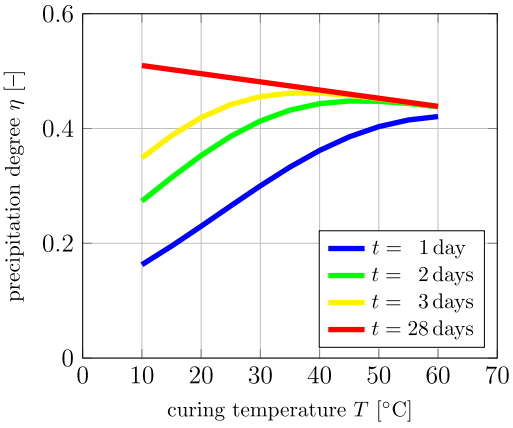


**Fig. 12.** Precipitation degree reached after $t = 1$ day (blue), $t = 2$ days (green), $t = 3$ days (yellow), and $t = 28$ days (red), as a function of curing temperature, according to the predictions of Eq. (31) and Table 4. (For interpretation of the references to color in this figure legend, the reader is referred to the web version of this article.)

## 4. Precipitation-driven constituent masses in the cement paste system, and corresponding degree of hydration

Having identified the precipitation degree as mix-, storage-, and temperature-invariant driver of all the hydrogen portions within a hydrating cement paste system, together with its temperature-dependent evolution characteristics, it is now time to relate the aforementioned hydrogen portions to all the constituents or phases which make up the investigated material system, as well as to the classical hydration degree. Starting with the hydrogen-containing phases, and denoting by $n_{H,j}$ the number of hydrogen atoms in one molecule of phase $j$, the mass of hydrogen-containing phase $j$ amounts to

$$m_j(t) = \frac{\mathcal{F}_{H,j}(t)}{n_{H,j}} M_j \, a_H(t) \,, \qquad j \in [CH, sCSH, gpor, cpor] \,, \tag{34}$$

with $M_j$ as the molar mass of phase $j$, i.e. the mass of one mole of phase $j$. The number of hydrogen atoms per molecule is constant in the case of calcium hydroxide and of the water filling the gel and capillary pores (see Table 6), while it depends on the curing temperature in the case of solid C-S-H, with the water-to-silica ratio $[(H_2O)/(SiO_2)](T)$ following Eq. (26). This leads to

$$n_{H,sCSH}(T) = n_{H,H_2O} \times 3.6327\big(\pi_5 \, T + \pi_6\big) \,. \tag{35}$$

Accordingly, the molar mass of solid C-S-H is temperature-dependent as well, in the following way,

$$M_{sCSH}(T) = M_{CS} + M_{H_2O} \times 3.6327\big(\pi_5 \, T + \pi_6\big) \,, \tag{36}$$

see also Table 6.

Turning to the only constituent which is free of hydrogen, namely clinker, we consider the beginning of the dissolution-precipitation reaction, with $\eta = 0$, when the initial water-to-cement mass ratio, $(w/c)$, gives access to the mass of clinker, through

$$\begin{aligned} m_{clin}(\eta=0) &= \frac{m_{H_2O}(\eta=0)}{(w/c)} = \frac{\mathcal{F}_{H,H_2O}(\eta=0)}{(w/c)} \frac{M_{H_2O}}{n_{H,H_2O}} a_H(\eta=0) \\ &= \frac{1}{(w/c)} \frac{M_{H_2O}}{n_{H,H_2O}} a_H(\eta=0) \,, \end{aligned} \tag{37}$$

whereby we have made use of Eq. (34) with $j = H_2O$, and of $\mathcal{F}_{H,H_2O}(\eta = 0) = 1$. At $\eta = 0$, the system consists only of water and clinker, so that the mass of overall cement paste follows as

$$m_{cp}(\eta=0) = \Big(1 + \frac{1}{(w/c)}\Big) m_{H_2O}(\eta=0) = \Big(1 + \frac{1}{(w/c)}\Big) \frac{M_{H_2O}}{n_{H,H_2O}} a_H(\eta=0) \,. \tag{38}$$

Under sealed conditions, $m_{cp}$ remains constant over time, so that Eq. (38) stays relevant also for any value $\eta$ beyond zero. However, when submerged under water, the cement paste system absorbs additional water molecules, as quantified in Section 2.4 in terms of the normalized hydrogen increase $\Delta I_H(\eta)$, see Eq. (23). Accordingly, the mass of cement paste is composed of its initial value (at zero precipitation degree) and the mass resulting from the water uptake,

$$m_{cp}(\eta) = m_{cp}(\eta=0) + \Delta I_H(\eta) \frac{M_{H_2O}}{n_{H,H_2O}} a_H(\eta=0) \,. \tag{39}$$

The initial amount of hydrogen can be expressed in terms of the mass of clinker and the initial water-to-cement mass ratio, by means of solving Eq. (37) for $a_H(\eta=0)$:

$$a_H(\eta=0) = m_{clin}(\eta=0) \times (w/c) \frac{n_{H,H_2O}}{M_{H_2O}} \,. \tag{40}$$

Insertion of Eq. (38) into Eq. (39), while considering Eq. (40), yields

$$m_{cp}(\eta) = \Big[1 + (w/c)\big(1 + \Delta I_H(\eta)\big)\Big] m_{clin}(\eta=0) \,, \tag{41}$$

with $\Delta I_H(\eta)$ according to Eq. (23), see also Table 3 for values of $\pi_4$ as a function of storage conditions. The mass of cement paste is also equal to the sum of the masses of all its constituents,

$$m_{cp}(\eta) = m_{clin}(\eta) + m_{gpor}(\eta) + m_{cpor}(\eta) + m_{sCSH}(\eta) + m_{CH}(\eta) \,, \tag{42}$$

whereby the masses of hydrogen-containing phases can be readily retrieved from the their specific masses according to Eq. (34), via

$$m_j(\eta) = \frac{\mathcal{F}_{H,j}(\eta)}{n_{H,j}} M_j \times a_H(\eta=0) \times \big(1 + \Delta I_H(\eta)\big) \,, \qquad j \in [CH, sCSH, gpor, cpor] \,. \tag{43}$$

Insertion of Eq. (40) into Eq. (43), and of the corresponding result and of Eq. (41), into Eq. (42) yields an equation for the mass of clinker, the solution of which yields

$$\begin{aligned} m_{clin}(\eta) \;=\; m_{clin}(\eta=0) \Bigg\{ 1 - \Bigg[ \big(\eta - \pi_1 \, \eta^{\pi_2}\big) \frac{M_{CH}}{n_{H,CH}} \frac{n_{H,H_2O}}{M_{H_2O}} + \\ \big(\pi_1 \, \eta^{\pi_2}\big)\Big(\frac{1}{3.6327\big(\pi_5 \, T + \pi_6\big)} \frac{M_{CS}}{M_{H_2O}} + 1\Big) - \eta \Bigg] (w/c)\big(1 + \pi_4 \, \eta\big) \Bigg\} \,, \end{aligned} \tag{44}$$

whereby we have made use of Eqs. (35), (36), and (26), Table 6, and Eq. (23), see also Table 3 for values of $\pi_4$ as a function of storage conditions. Insertion of Eq. (44) into Eq. (2) delivers the hydration degree as a function of the precipitation degree, in the format

$$\begin{aligned} \xi(\eta) = (w/c)\big(1 + \pi_4 \, \eta\big) \Bigg[ \big(\eta - \pi_1 \, \eta^{\pi_2}\big)\Big(\frac{M_{CH}}{M_{H_2O}} \frac{n_{H,H_2O}}{n_{H,CH}} - 1\Big) \\ + \frac{\pi_1 \, \eta^{\pi_2}}{3.6327\big(\pi_5 \, T + \pi_6\big)} \frac{M_{CS}}{M_{H_2O}} \Bigg] \,, \end{aligned} \tag{45}$$

with $\pi_4 = 0$ for the sealed case and with $\pi_4 = 0.1880$ for under water curing, according to Table 3. For any specific value of the precipitation

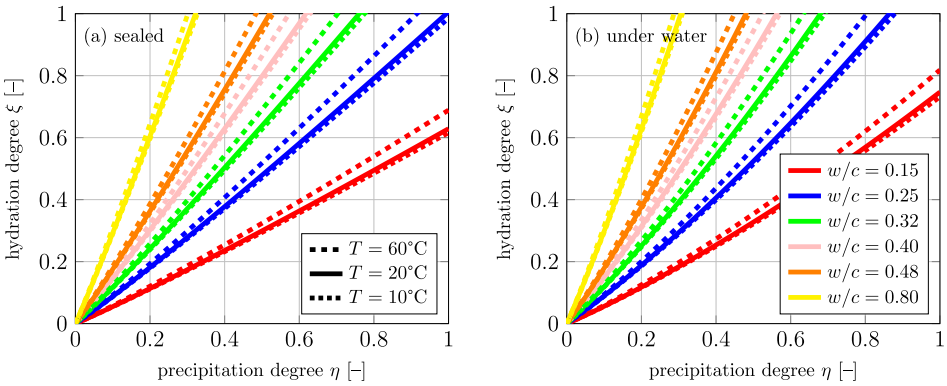


**Fig. 13.** Hydration degrees as functions of the precipitation degree, according to Eq. (45), for cement pastes with initial water-to-cement mass ratios $w/c = 0.15$ (red), $w/c = 0.24$ (blue), $w/c = 0.32$ (green), $w/c = 0.40$ (pink), $w/c = 0.48$ (orange), and $w/c = 0.80$ (yellow); $T = 10$ °C (dotted lines), $T = 20$ °C (solid lines), and $T = 60$ °C (dashed lines); cured (a) under sealed conditions, and (b) under water. (For interpretation of the references to color in this figure legend, the reader is referred to the web version of this article.)

**Table 7**
Mass densities of water, calcium hydroxide, and clinker [17].

| | Water | Calcium hydroxide | Clinker |
|---|---|---|---|
| mass density [g/cm$^3$] | $\rho_{H_2O} = 1.00$ | $\rho_{CH} = 2.24$ | $\rho_{clin} = 3.15$ |

degree, the associated value of the hydration degree is the larger, the larger the initial water-to-cement mass ratio and the larger the curing temperature, see Fig. 13 and note that $\pi_5$ in Eq. (45) is negative, see Table 4. Also, the associated value of the hydration degree is larger in under-water-cured samples than in sealed-cured samples, and this difference increases with decreasing initial water-to-cement mass ratio.

## 5. Precipitation-driven constituent volumes of the cement paste system, and corresponding mass density of solid C-S-H

### 5.1. Volumes of invariably dense material constituents and of overall cement paste

Determination of volumes from masses require the knowledge of mass densities. The latter are constant for all phases except solid C-S-H, the mass density of which has been reported to depend on temperature and maturity [20,29]. Thus, the volumes occupied by every phase except solid C-S-H are obtained from dividing their masses $m_j(t)$, from Eqs. (43) and (44), by their mass densities $\rho_j$:

$$V_j(\eta) = \frac{m_j(\eta)}{\rho_j}\,, \qquad j \in [clin, CH, gpor, cpor]\,, \tag{46}$$

where $\rho_{gpor} = \rho_{cpor} = \rho_{H_2O}$, see Table 7 for numerical values.

Irrespective of the storage conditions (i.e. under water or selaed), the total volume of cement paste $V_{cp}$ may be treated as being virtually constant throughout hardening, because bulk volume changes at the macroscopic scale of cement paste are by two orders of magnitude smaller than chemical shrinkage [36,37]. Thus, $V_{cp}$ is set equal to the initial volume of cement paste, i.e. to the sum of the initial volumes of water and clinker. Under consideration of Eqs. (46) and of $(w/c) = m_{H_2O}(\eta{=}0)/m_{clin}(\eta{=}0)$, this yields

$$V_{cp} = V_{cp}(\eta{=}0) = V_{H_2O}(\eta{=}0) + V_{clin}(\eta{=}0) = m_{clin}(\eta{=}0)\left[\frac{(w/c)}{\rho_{H_2O}} + \frac{1}{\rho_{clin}}\right]. \tag{47}$$

The constituent volumes according to Eq. (46), together with Eqs. (43) and (44), and the volume of cement paste according to Eq. (47) give access to the volume fractions of the phases with invariable mass density, $f_j = V_j/V_{cp}$, in the form

$$f_{clin} = \left\{ 1 + (w/c)(1+\pi_4\,\eta) - \left[ (\eta - \pi_1\,\eta^{\pi_2}) \frac{M_{CH}}{n_{H,CH}} \frac{n_{H,H_2O}}{M_{H_2O}} + (1-\eta) + (\pi_1\,\eta^{\pi_2}) \left( \frac{1}{3.6327(\pi_5\,T + \pi_6)} \frac{M_{CS}}{M_{H_2O}} + 1 \right) \right] (w/c)(1+\pi_4\,\eta) \right\} \left[ \frac{(w/c)\rho_{clin}}{\rho_{H_2O}} + 1 \right]^{-1}, \tag{48}$$

$$f_{CH} = \frac{n_{H,H_2O}}{M_{H_2O}} \frac{M_{CH}}{n_{H,CH}} (\eta - \pi_1\,\eta^{\pi_2})(1+\pi_4\,\eta) \left[ \frac{\rho_{CH}}{\rho_{H_2O}} + \frac{\rho_{CH}}{(w/c)\rho_{clin}} \right]^{-1}, \tag{49}$$

$$f_{gpor} = \begin{cases} (1-\eta)(\pi_3\,\eta)(1+\pi_4\,\eta) \left[ 1 + \frac{\rho_{H_2O}}{(w/c)\rho_{clin}} \right]^{-1} & \dots\ \eta \le 1/\pi_3\,, \\ (1-\eta)(1+\pi_4\,\eta) \left[ 1 + \frac{\rho_{H_2O}}{(w/c)\rho_{clin}} \right]^{-1} & \dots\ \eta > 1/\pi_3\,, \end{cases} \tag{50}$$

$$f_{cpor} = \begin{cases} (1-\eta)(1-\pi_3\,\eta)(1+\pi_4\,\eta) \left[ 1 + \frac{\rho_{H_2O}}{(w/c)\rho_{clin}} \right]^{-1} & \dots\ \eta \le 1/\pi_3\,, \\ 0 & \dots\ \eta > 1/\pi_3\,. \end{cases} \tag{51}$$

The remaining volume fraction, complementing the sum of Eqs. (48) to (51) to one, is associated to solid C-S-H and vapor-filled voids in the case of sealed curing, and by solid C-S-H only in the case of under water curing.

### 5.2. Determination of mass density of solid C-S-H , from under water cured samples

For under-water-cured samples, the total volume of cement paste is made up of the volumes of clinker, of calcium hydroxide, of gel pores and capillary pores, and of solid C-S-H. Hence, the latter volume can be computed from

$$V_{sCSH}(\eta, T) = V_{cp} - \left[ V_{clin}(\eta, T) + V_{CH}(\eta) + V_{gpor}(\eta) + V_{cpor}(\eta) \right]. \tag{52}$$

This volume allows for determination of both the volume fraction of solid C-S-H in under-water-cured samples, as

$$f_{sCSH} = \frac{V_{sCSH}}{V_{cp}} = 1 - \left[ f_{clin} + f_{CH} + f_{gpor} + f_{cpor} \right], \tag{53}$$

see Fig. 15, and of the mass density of solid C-S-H, $\rho_{sCSH} = \frac{m_{sCSH}}{V_{sCSH}}$, as

$$\rho_{sCSH} = \left( \frac{M_{sCSH}(T)}{n_{H,sCSH}(T)} \pi_1\,\eta^{\pi_2} \right) \left\{ \frac{M_{H_2O}}{n_{H,H_2O}} \left[ \frac{1}{\rho_{H_2O}} \left( \frac{1}{1 + 0.188\,\eta} + \eta - 1 \right) - \frac{\eta}{\rho_{clin}} \right] + \left( \frac{1}{\rho_{clin}} - \frac{1}{\rho_{CH}} \right) \frac{M_{CH}}{n_{H,CH}} (\eta - \pi_1\,\eta^{\pi_2}) + \frac{1}{\rho_{clin}} \frac{M_{sCSH}(T)}{n_{H,sCSH}(T)} \pi_1\,\eta^{\pi_2} \right\}^{-1}, \tag{54}$$

where $\pi_4$ was set equal to 0.188, and whereby we have made use of Eqs. (52), (47), (46), (44), (43), (13), (14), (19), and (20), see Fig. 14. We note that the mass density of solid C-S-H decreases with increasing precipitation degree and with decreasing temperature, while

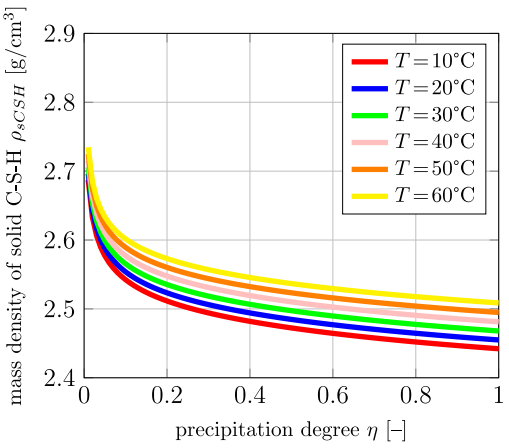


**Fig. 14.** Density of solid C-S-H in cement pastes cured under water and isothermally at: $T$ = 10 °C (red), $T$ = 20 °C (blue), $T$ = 30 °C (green), $T$ = 40 °C (pink), $T$ = 50 °C (orange), and $T$ = 60 °C (yellow); from Eq. (54). (For interpretation of the references to color in this figure legend, the reader is referred to the web version of this article.)

being independent of the initial water-to-cement mass ratio; and the corresponding range of values agrees very well with the range of values reported in the open literature [17,20,25,28,29,38,39].

### 5.3. Volume fractions in cement paste precipitating under sealed conditions

When considering that the precipitation- and temperature-dependence of the mass density of solid C-S-H according to Fig. 14 and Eq. (54) holds also for sealed curing conditions, the volume occupied by solid C-S-H is obtained as

$$V_{sCSH}(\eta,T) = \frac{m_{sCSH}(\eta,T)}{\rho_{sCSH}(\eta,T)}\,, \tag{55}$$

with the mass of solid C-S-H following Eq. (43), with $\pi_4 = 0$, expressing sealed conditions, see Table 3; and with the mass density of solid C-S-H following Eq. (54), expressing that the mass density of solid C-S-H does not depend on storage conditions. This yields

$$\begin{aligned} V_{sCSH}(\eta,T) \;=\; & m_{clin}(\eta{=}0)\times(w/c)\left[\frac{1}{\rho_{\mathrm{H_2O}}}\left(\frac{1}{1+0.188\,\eta}+\eta-1\right)-\frac{\eta}{\rho_{clin}}\right.\\ & +\left(\frac{1}{\rho_{clin}}-\frac{1}{\rho_{CH}}\right)\frac{M_{CH}}{n_{H,CH}}\frac{n_{H,\mathrm{H_2O}}}{M_{\mathrm{H_2O}}}\left(\eta-\pi_1\,\eta^{\pi_2}\right)\\ & \left.+\frac{1}{\rho_{clin}}\left(\frac{1}{3.6327\left(\pi_5\,T+\pi_6\right)}\frac{M_{CS}}{M_{\mathrm{H_2O}}}+1\right)\pi_1\,\eta^{\pi_2}\right]\,. \end{aligned} \tag{56}$$

We are left with the determination of the volume filled by voids resulting from chemical shrinkage under sealed conditions, based on representing the overall cement paste volume as the sum of the volumes of all phases, and solving this volume accumulation equation for $V_{void}$. Mathematically, this reads as

$$V_{void}(\eta) = V_{cp} - \Big[V_{clin}(\eta,T) + V_{CH}(\eta) + V_{sCSH}(\eta,T) + V_{gpor}(\eta) + V_{cpor}(\eta)\Big]\,, \tag{57}$$

whereby the volume expressions on the right-hand side of Eq. (57) follow from Eqs. (47), (46), (56), (44), (43), (13), (14), (19), and (20), so that the temperature dependence vanishes. Thus, the volume fractions of calcium hydroxide, of gel and capillary pores, and of clinker in sealed samples follow from Eqs. (48)–(51), for $\pi_4 = 0$, see Table 3. The volume fraction of solid C-S-H, in turn, follows from dividing Eq. (56) by Eq. (47), yielding

$$\begin{aligned} f_{sCSH}^{seal} \;=\; & \left[\frac{1}{\rho_{\mathrm{H_2O}}}\left(\frac{1}{1+0.188\,\eta}+\eta-1\right)-\frac{\eta}{\rho_{clin}}\right.\\ & +\left(\frac{1}{\rho_{clin}}-\frac{1}{\rho_{CH}}\right)\frac{M_{CH}}{n_{H,CH}}\frac{n_{H,\mathrm{H_2O}}}{M_{\mathrm{H_2O}}}\left(\eta-\pi_1\,\eta^{\pi_2}\right)\\ & \left.+\frac{1}{\rho_{clin}}\left(\frac{1}{3.6327\left(\pi_5\,T+\pi_6\right)}\frac{M_{CS}}{M_{\mathrm{H_2O}}}+1\right)\pi_1\,\eta^{\pi_2}\right]\\ & \left[\frac{1}{\rho_{\mathrm{H_2O}}}+\frac{1}{(w/c)\rho_{clin}}\right]^{-1}\,, \end{aligned} \tag{58}$$

where $\rho_{sCSH}(\eta,T)$ was taken from Eq. (54). Finally, the volume fraction of voids reads as

$$f_{void} = 1 - \Big[f_{clin} + f_{CH} + f_{gpor} + f_{cpor} + f_{sCSH}^{seal}\Big]\,, \tag{59}$$

see Fig. 15.

As discussed in Section 4, the precipitation degree and the hydration degree are uniquely related, see Eq. (45). Therefore, the derived volume fractions can be also expressed in terms of the hydration degree, see Fig. 16.

## 6. Discussion and conclusion

We have presented a new cement hydration model which explicitly accounts for the increasing evidence that hydration is a combined dissolution-precipitation process [8–12]. Accordingly, the formation of calcium hydroxide and C-S-H is quantified through a precipitation degree defined, from proton NMR data [17,20], as the amount of bound hydrogen over the total amount of hydrogen found in a hydrating cement paste sample. As the only functional argument, fully independent of mix proportions, of storage characteristics (sealed versus under water curing), and of curing temperature, the precipitation degree governs the hydrogen molar fractions associated with the gel and capillary porosities, as well as with calcium hydroxide and solid C-S-H. Moreover, the precipitation degree provides temperature-independent linear water uptake characteristics, as driven by chemical shrinkage of cement pastes.

In this context, it seems appropriate to discuss the source of the aforementioned molar fractions of differently bound hydrogen in the cement paste systems, i.e. the identification of differently strongly bound hydrogen populations from NMR experiments: From a historical perspective, Holly et al. [40] were the first to resolve four hydrogen populations in white cement paste systems, and their partition of the hydrogen into different groups is in full consistency with the results provided by Muller et al. [17] and Gajewicz et al. [20], used in the present contribution; as well as with the study of Bahafid et al. [29] on class G cements, referred to in more detail further below. In contrast to these results, Muller et al. [17] report that earlier studies either lacked the temporal resolution to see the fastest relaxing components, e.g. calcium hydroxide-bound hydrogen, or failed to separately resolve the protons in solid C-S-H and gel pores.

Apart from these mix-, storage-, and temperature-invariances, the precipitation degree also provides an interesting complement to pertinent hydration degree-based kinetics modeling [31,41,42]; namely through consideration of the temperature-driven stoichiometry of solid C-S-H, a characteristic which has become more and more evident in recent years [28,29]: Hydration products arising in pastes cured isothermally under different temperatures exhibit a water-to-silica ratio which decreases with increasing temperature; and such a loss of water bound to calcium-silicate is even recorded when changing the temperature of cement pastes at a constant maturation state, resulting in water redistributions towards the gel and capillary porosities [43], as well as to the vapor-filled voids in the context of hygrothermal effects [44]. Accordingly, we have normalized the precipitation degree by its temperature-dependent maximum, and this normalized quantity turns out to be governed by a thermally activated Arrhenius-type reaction. The latter is characterized by a simple, linear affinity function, as normally expected in standard physical chemistry applications. We note that pertinent kinetics modeling approaches based on the degree of hydration required the introduction of a more complex, non-linear affinity

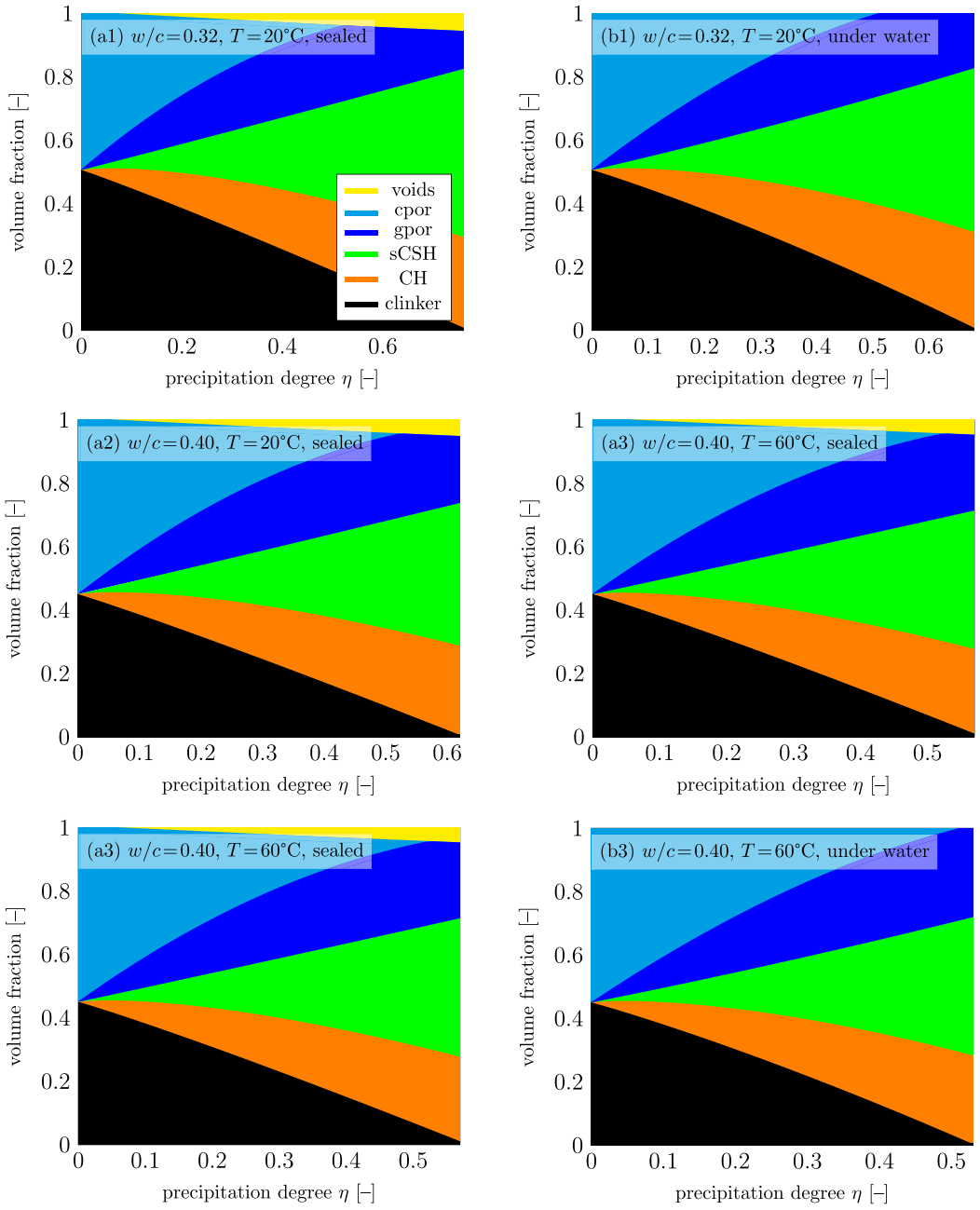


**Fig. 15.** Evolution of phase assemblage of cement pastes with (1) $w/c = 0.32$ and (2,3) $w/c = 0.40$; cured at (1,2) $T = 20$ °C and (3) $T = 60$ °C; stored (a) under sealed conditions and (b) under water, as functions of the precipitation degree. (For interpretation of the references to color in this figure legend, the reader is referred to the web version of this article.)

function [26,30,31], indicating the presence of quite distinct chemical processes having been, somewhat arbitrarily, lumped together.

Finally, mass and volume balancing shows that the mass density of solid C-S-H is dependent on both the precipitation degree and the curing temperature, spanning over a range of numerical values which is fully consistent with the variations known between earlier estimations provided in the open literature, encompassing values from 2.5 g/cm$^3$ [29,39], via 2.6 g/cm$^3$ [25,38] to 2.7 g/cm$^3$ [17,20]; and similar balancing considerations provide also links between the precipitation degree introduced in the present paper, and the classical hydration degree, as well as the volume fractions of material constituents. The latter allow for linking the novel developments presented herein with the rich world of micromechanical modeling [4,6,45–47]; especially to models accounting for different pore structures and hydrate densification [48,49]. Over the last two decades, such models have become major theoretical and computational tools for innovative concrete design.

The aforementioned link between precipitation degree and hydration degree was derived on the basis of a curing temperature-independent calcium-to-silica ratio in solid C-S-H. This independence was shown by combination of NMR, X-ray diffraction (XRD), and thermogravimetry (TGM) data, with mass, volume and oxides balance equations [20,28], in consistency with the calcium-to-silica ratio of 1.7 evidenced from combining small-angle neutron and X-ray scattering (SAXS and SANS) data, and by exploiting the hydrogen/deuterium neutron isotope effect both in water and methanol [25]. In this context, it is interesting to note that in a cement paste system which is different from the one analyzed here, namely in a class G oil-well cement (also

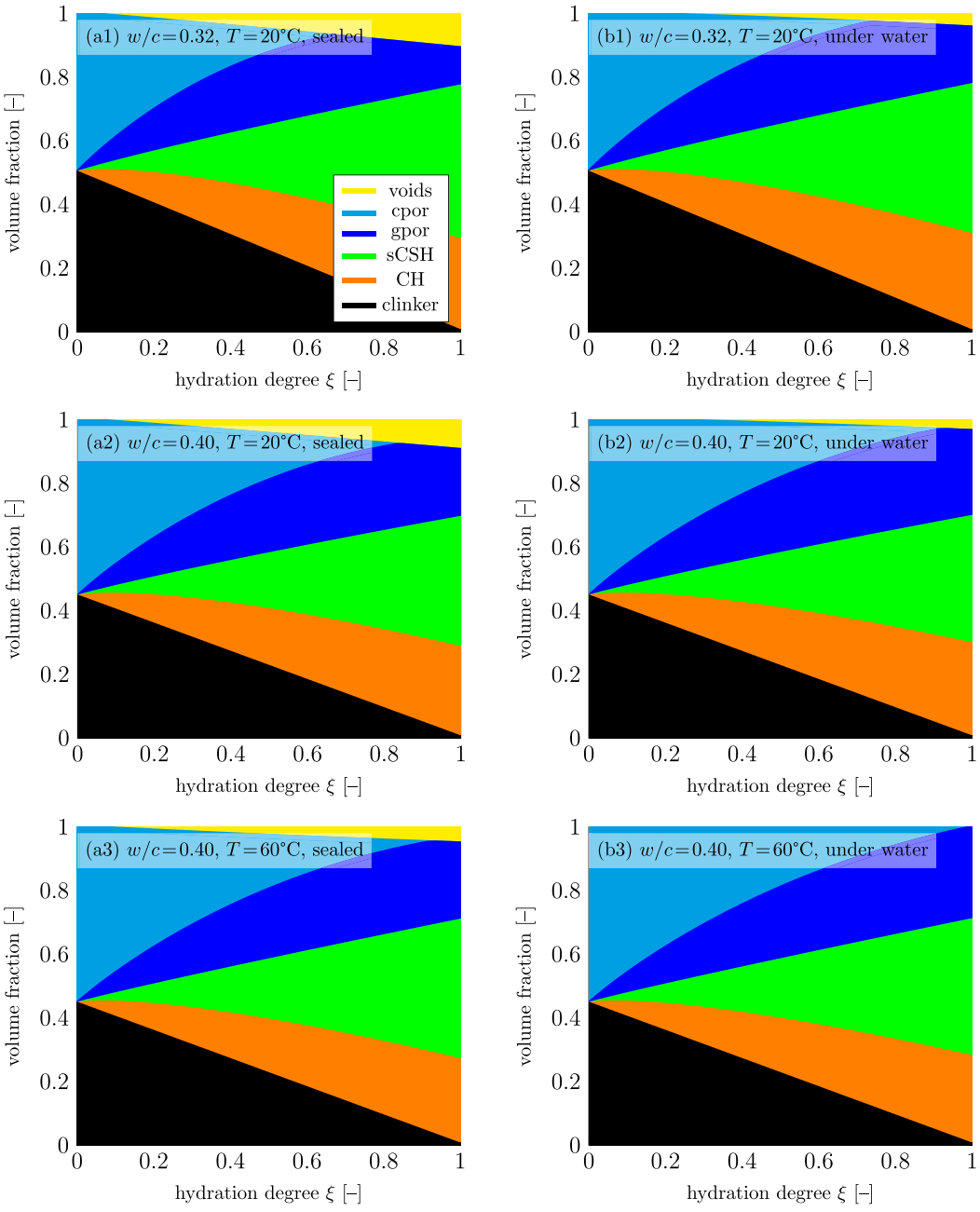


**Fig. 16.** Evolution of phase assemblage of cement pastes with (1) $w/c = 0.32$ and (2,3) $w/c = 0.40$; cured at (1,2) $T = 20$ °C and (3) $T = 60$ °C; stored (a) under sealed conditions and (b) under water, as functions of the hydration degree. (For interpretation of the references to color in this figure legend, the reader is referred to the web version of this article.)

characterized by XRD, TGM, and balance equations), the calcium-to-silica ratio might well decrease with increasing curing temperature between 0 and 100 centigrades, ranging then from 1.93 to 1.7 [29]. For the study of such a system, our approach would need to undergo only relatively slight modifications. Namely, the molar mass of the calcium-silicate in C-S-H, $M_{CS}$, in Eq. (36) would become temperature dependent, i.e.

$$M_{CS}(T) = M_S + M_C \times [(\mathrm{CaO})/(\mathrm{SiO_2})](T)\,, \tag{60}$$

where the molar mass of silicate is $M_S = 60.1\,\mathrm{g/mol}$, the molar mass of calcium oxide is $M_C = 56.1\,\mathrm{g/mol}$, and $[(\mathrm{CaO})/(\mathrm{SiO_2})](T)$ refers to the temperature-dependent calcium-to-silica ratio. The introduced temperature-dependence of the calcium-to-silica ratio would affect the relation between the precipitation degree and the hydration degree, see Eq. (45), as well as the mass density of solid C-S-H, see Eq. (54). However, numerical evaluations of class G cements with such a modified model go beyond the scope of the present contribution.

Conclusively, the proton-NMR-derived mix-, storage-, and temperature-invariant relations between the herein newly introduced precipitation degree and the molar fractions of hydrogen found in capillary and gel pores, as well as in solid C-S-H and portlandite, further confirm the existence and chemical relevance of four different

hydrogen populations in cement paste, as probably first discovered by Holly et al. [40]. Moreover, the consistency of the evolution of this precipitation degree with a linearly decreasing chemical affinity function, in full consistency with classical physical chemistry [34], further confirms the eminent importance of the hydrate precipitation process in the overall hydration process, the latter being then seen as a coupled dissolution-precipitation process [50].

## CRediT authorship contribution statement

**Nabor Jiménez Segura:** Conceptualization, Investigation, Formal analysis, Software, Methodology, Writing – original draft, Writing – review & editing. **Bernhard L.A. Pichler:** Conceptualization, Investigation, Methodology, Project administration, Funding acquisition, Supervision, Validation, Writing – original draft, Writing – review & editing. **Christian Hellmich:** Conceptualization, Investigation, Methodology, Resources, Supervision, Validation, Writing – original draft, Writing – review & editing.

## Declaration of competing interest

The authors declare that they have no known competing financial interests or personal relationships that could have appeared to influence the work reported in this paper.

## Data availability

All data are from published sources and explicitly given in the article.

## Acknowledgments

The authors gratefully acknowledge financial support in the framework of the European Union's Horizon 2020 research and innovation programme under the Marie Skłodowska-Curie grant agreement No. 764691.

## Appendix. NMR testing of cement pastes at different temperatures by Gajewicz et al. [19,20]

Proton NMR tests were performed on a permanent bench-top NMR magnet equipped with a Kea2 (Magritek, New Zealand) NMR spectrometer, at 20 MHz frequency. They allowed for recording of quadrature "solid" [51] and Carr-Purcell-Meiboom-Gill (CPMG) [52,53] echo trains. Both 90° and 180° excitation pulses exhibited a duration of 5 μs, while the intensity of the 180° pulses exceed those of the 90° pulses by a factor of two. The CPGM decay data were evaluated by a constrained exponential stripping method, see [20] for further details.

As regards cement paste preparation, we cite from [20]: *"Distilled water was added to 80 g of anhydrous powder. Pastes were mixed for 3 min at 500 rpm, rested for 2 min and then further mixed for 2 min at 2000 rpm. Immediately after mixing, aliquots of paste of circa 0.4 $cm^3$ were inserted into 10 mm outside diameter NMR tubes using a plastic pipette. [. . . ] A few drops of saturated calcium hydroxide (CH) solution were added on the top of pastes for "underwater" curing. The NMR tubes and larger containers were tightly closed using parafilm®".*

## References

[1] A.M. Neville, Properties of Concrete, fourth ed., Longman, London, 1995.
[2] P. Acker, Micromechanical analysis of creep and shrinkage mechanisms, in: Creep, Shrinkage and Durability Mechanics of Concrete and Other Quasi-Brittle Materials (Proceedings of ConCreep-6@ MIT), Elsevier, Amsterdam, 2001, pp. 15–26.
[3] M. Mouret, A. Bascoul, G. Escadeillas, Study of the degree of hydration of concrete by means of image analysis and chemically bound water, Adv. Cem. Based Mater. 6 (1997) 109–115.
[4] O. Bernard, F.-J. Ulm, E. Lemarchand, A multiscale micromechanics-hydration model for the early-age elastic properties of cement-based materials, Cem. Concr. Res. 33 (2003) 1293–1309.
[5] X. Feng, E.J. Garboczi, D.P. Bentz, P.E. Stutzman, T.O. Mason, Estimation of the degree of hydration of blended cement pastes by a scanning electron microscope point-counting procedure, Cem. Concr. Res. 34 (2004) 1787–1793.
[6] C. Hellmich, H. Mang, Shotcrete elasticity revisited in the framework of continuum micromechanics: From submicron to meter level, J. Mater. Civ. Eng. 17 (2005) 246–256.
[7] M. Königsberger, C. Hellmich, B. Pichler, Densification of C-S-H is mainly driven by available precipitation space, as quantified through an analytical cement hydration model based on NMR data, Cem. Concr. Res. 88 (2016) 170–183.
[8] J.W. Bullard, H.M. Jennings, R.A. Livingston, A. Nonat, G.W. Scherer, J.S. Schweitzer, K.L. Scrivener, J.J. Thomas, Mechanisms of cement hydration, Cem. Concr. Res. 41 (2011) 1208–1223.
[9] K.L. Scrivener, A. Nonat, Hydration of cementitious materials, present and future, Cem. Concr. Res. 41 (2011) 651–665.
[10] K. Ioannidou, K.J. Krakowiak, M. Bauchy, C.G. Hoover, E. Masoero, S. Yip, F.-J. Ulm, P. Levitz, R.J.-M. Pellenq, E. Del Gado, Mesoscale texture of cement hydrates, Proc. Natl. Acad. Sci. 113 (2016) 2029–2034.
[11] T. Powers, Absorption of water by Portland cement paste during the hardening process, Ind. Eng. Chem. 27 (1935) 790–794.
[12] C. Hua, A. Ehrlacher, P. Acker, Analyses and models of the autogenous shrinkage of hardening cement paste II. Modelling at scale of hydrating grains, Cem. Concr. Res. 27 (1997) 245–258.
[13] A.R. Brough, C.M. Dobson, I.G. Richardson, G.W. Groves, Application of selective 29Si isotopic enrichment to studies of the structure of calcium silicate hydrate (C-S-H) gels, J. Am. Ceram. Soc. 77 (1994) 593–596.
[14] H.M. Jennings, J.W. Bullard, J.J. Thomas, J.E. Andrade, J.J. Chen, G.W. Scherer, Characterization and modeling of pores and surfaces in cement paste, J. Adv. Concr. Technol. 6 (2008) 5–29.
[15] H.M. Jennings, Refinements to colloid model of C-S-H in cement: CM-II, Cem. Concr. Res. 38 (2008) 275–289.
[16] P.J. McDonald, V. Rodin, A. Valori, Characterisation of intra- and inter-C–S–H gel pore water in white cement based on an analysis of NMR signal amplitudes as a function of water content, Cem. Concr. Res. 40 (2010) 1656–1663.
[17] A.C.A. Muller, K.L. Scrivener, A.M. Gajewicz, P.J. McDonald, Densification of C–S–H measured by 1H NMR relaxometry, J. Phys. Chem. C 117 (2013) 403–412.
[18] A.C.A. Muller, Characterization of Porosity & C-S-H in Cement Pastes By 1H NMR (Ph.D. thesis), 2014.
[19] A.M. Gajewicz, Characterisation of Cement Microstructure and Pore-Water Interaction By 1H Nuclear Magnetic Resonance Relaxometry (Ph.D. thesis), 2014.
[20] A.M. Gajewicz-Jaromin, P.J. McDonald, A.C.A. Muller, K.L. Scrivener, (Ph.D. thesis), Influence of curing temperature on cement paste microstructure measured by 1H NMR relaxometry Cem. Concr. Res. 122 (2019) 147–156.
[21] H. Le Châtelier, Sur les changements de volume qui accompagnent le durcissement des ciments [on the changes in volume which accompany the hardening of cement], Bull. Soc. L'Encouragement Pour L'Industrie Nationale 5 (5) (1900) 54–57.
[22] E.-I. Tazawa, S. Miyazawa, T. Kasai, Chemical shrinkage and autogenous shrinkage of hydrating cement paste, Cem. Concr. Res. 25 (1995) 288–292.
[23] P. Lura, J. Couch, O.M. Jensen, J. Weiss, Early-age acoustic emission measurements in hydrating cement paste: Evidence for cavitation during solidification due to self-desiccation, Cem. Concr. Res. 39 (2009) 861–867.
[24] A. Valori, P.J. McDonald, K.L. Scrivener, The morphology of C–S–H: Lessons from 1H nuclear magnetic resonance relaxometry, Cem. Concr. Res. 49 (2013) 65–81.
[25] A.J. Allen, J.J. Thomas, H.M. Jennings, Composition and density of nanoscale calcium–silicate–hydrate in cement, Nature Mater. 6 (2007) 311–316.
[26] C. Hellmich, F.-J. Ulm, H.A. Mang, Multisurface chemoplasticity. I: Material model for shotcrete, J. Eng. Mech. 125 (1999) 692–701.
[27] L. D'Aloia, G. Chanvillard, Determining the apparent activation energy of concrete: Ea—numerical simulations of the heat of hydration of cement, Cem. Concr. Res. 32 (2002) 1277–1289.
[28] E. Gallucci, X. Zhang, K.L. Scrivener, Effect of temperature on the microstructure of calcium silicate hydrate (C-S-H), Cem. Concr. Res. 53 (2013) 185–195.
[29] S. Bahafid, S. Ghabezloo, M. Duc, P. Faure, J. Sulem, Effect of the hydration temperature on the microstructure of Class G cement: C-S-H composition and density, Cem. Concr. Res. 95 (2017) 270–281.
[30] F.-J. Ulm, O. Coussy, Strength growth as chemo-plastic hardening in early age concrete, J. Eng. Mech. 122 (1996) 1123–1132.
[31] C. Hellmich, F.-J. Ulm, H.A. Mang, Consistent linearization in Finite Element analysis of coupled chemo-thermal problems with exo- or endothermal reactions, Comput. Mech. 24 (1999) 238–244.
[32] P. Termkhajornkit, R. Barbarulo, Modeling the coupled effects of temperature and fineness of Portland cement on the hydration kinetics in cement paste, Cem. Concr. Res. 42 (2012) 526–538.
[33] S. Arrhenius, Über die Reaktionsgeschwindigkeit bei der Inversion von Rohrzucker durch Sären, Z. Phys. Chem. 4U (1889) 226–248.
[34] P. Atkins, P.W. Atkins, J.D. Paula, Atkins' Physical Chemistry, OUP, Oxford, 2014.

[35] G.J. Verbeck, Structures and physical properties of cement paste, in: 5th International Congress on the Chemistry of Cement, 1968, Vol. 3, 1968, pp. 1–37.
[36] P. Lura, O.M. Jensen, K. Van Breugel, Autogenous shrinkage in high-performance cement paste: An evaluation of basic mechanisms, Cem. Concr. Res. 33 (2003) 223–232.
[37] M. Abuhaikal, K. Ioannidou, T. Petersen, R.J.M. Pellenq, F.-J. Ulm, Le Châtelier's conjecture: Measurement of colloidal eigenstresses in chemically reactive materials, J. Mech. Phys. Solids 112 (2018) 334–344.
[38] H.F. Taylor, Proposed structure for calcium silicate hydrate gel, J. Am. Ceram. Soc. 69 (1986) 464–467.
[39] G. Constantinides, F.-J. Ulm, The effect of two types of C-S-H on the elasticity of cement-based materials: Results from nanoindentation and micromechanical modeling, Cem. Concr. Res. 34 (2004) 67–80.
[40] R. Holly, E. Reardon, C. Hansson, H. Peemoeller, Proton spin–spin relaxation study of the effect of temperature on white cement hydration, J. Am. Ceram. Soc. 90 (2007) 570–577.
[41] G. De Schutter, L. Taerwe, General hydration model for Portland cement and blast furnace slag cement, Cem. Concr. Res. 25 (1995) 593–604.
[42] F.-J. Ulm, O. Coussy, Modeling of thermochemomechanical couplings of concrete at early ages, J. Eng. Mech. 121 (1995) 785–794.
[43] M. Wyrzykowski, P.J. McDonald, K.L. Scrivener, P. Lura, Water redistribution within the microstructure of cementitious materials due to temperature changes studied with 1H NMR, J. Phys. Chem. C 121 (2017) 27950–27962.
[44] H. Wang, C. Hellmich, Y. Yuan, H. Mang, B. Pichler, May reversible water uptake/release by hydrates explain the thermal expansion of cement paste? — Arguments from an inverse multiscale analysis, Cem. Concr. Res. 113 (2018) 13–26.
[45] J. Sanahuja, L. Dormieux, G. Chanvillard, Modelling elasticity of a hydrating cement paste, Cem. Concr. Res. 37 (2007) 1427–1439.
[46] B. Pichler, C. Hellmich, Upscaling quasi-brittle strength of cement paste and mortar: A multi-scale engineering mechanics model, Cem. Concr. Res. 41 (2011) 467–476.
[47] M. Königsberger, M. Hlobil, B. Delsaute, S. Staquet, C. Hellmich, B. Pichler, Hydrate failure in ITZ governs concrete strength: A micro-to-macro validated engineering mechanics model, Cem. Concr. Res. 103 (2018) 77–94.
[48] S. Bahafid, S. Ghabezloo, P. Faure, M. Duc, J. Sulem, Effect of the hydration temperature on the pore structure of cement paste: Experimental investigation and micromechanical modelling, Cem. Concr. Res. 111 (2018) 1–14.
[49] M. Königsberger, B. Pichler, C. Hellmich, Multiscale poro-elasticity of densifying calcium-silicate hydrates in cement paste: An experimentally validated continuum micromechanics approach, Internat. J. Engrg. Sci. 147 (2020) 103196.
[50] L. Nicoleau, A. Nonat, A new view on the kinetics of tricalcium silicate hydration, Cem. Concr. Res. 86 (2016) 1–11.
[51] J. Powles, J. Strange, Zero time resolution nuclear magnetic resonance transient in solids, Proc. Phys. Soc. 82 (1963) 6.
[52] H.Y. Carr, E.M. Purcell, Effects of diffusion on free precession in nuclear magnetic resonance experiments, Phys. Rev. 94 (1954) 630.
[53] S. Meiboom, D. Gill, Modified spin-echo method for measuring nuclear relaxation times, Rev. Sci. Instrum. 29 (1958) 688–691.